Magazine of Concrete Research
Volume 63 Issue 5

Analysis of hydration heat and autogenous shrinkage of high-strength mass concrete
Kim, Lee, Nam and Koo

Magazine of Concrete Research, 2011, **63**(5), 377–389
doi: 10.1680/macr.9.00106
Paper 900106
Received 22/06/2009; revised 03/06/2010; accepted 16/06/2010
Published online ahead of print 12/04/2011

ice
Institution of Civil Engineers
publishing

Analysis of hydration heat and autogenous shrinkage of high-strength mass concrete

Gyu-Yong Kim
Department of Architectural Engineering, Chungnam National University, Deajoen, South Korea

Eui-Bae Lee
Daewoo Institute of Construction Technology, Suwon, South Korea

Jeong-Soo Nam
Department of Architectural Engineering, Chungnam National University, Deajoen, South Korea

Kyung-Mo Koo
Department of Architectural Engineering, Chungnam National University, Deajoen, South Korea

The early-age properties and relationships between hydration heat and autogenous shrinkage in high-strength mass concrete of different mixture proportions are investigated through analysis of the history curves of hydration heat and autogenous shrinkage. The hydration temperature and hydration heating velocity (HHV) of the concrete were found to increase with increases in specimen size and decrease when the concrete contained a retarder, fly ash (FA) and ground granulated blast-furnace slag (GGBS). Even in samples of the same mixture proportion, autogenous shrinkage was noted to become greater as the inner temperature increased. The autogenous shrinkage of high-strength mass concrete containing FA and GGBS was lower than that of ordinary Portland cement high-strength mass concrete. The autogenous shrinking velocity of concrete increased as the size of the specimen increased and decreased when the concrete contained a retarder, FA and GGBS. Finally, a close correlation was found between the hydration temperature and autogenous shrinkage at an early age: a higher HHV and a larger HHV–maturity factor led to greater autogenous shrinkage.

Introduction

In high-strength mass concrete, low water/cement (w/c) or water/binder (w/b) ratios lead to significant self-desiccation during hydration (Lura *et al.*, 2003); its hydration heat and low thermal conductivity also lead to a high inner temperature. High-strength mass concrete therefore experiences both enormous autogenous shrinkage and high hydration heat at an early age. Bjøntegaard *et al.* (1997) and Horita and Nawa (2001) reported that the magnitude and rate of development of autogenous shrinkage depend strongly on the temperature history of the concrete since it was first mixed. Loukili *et al.* (2000) and Shima *et al.* (2006) found that autogenous shrinkage increases at high temperature for the same mortar or concrete compositions. Most autogenous shrinkage of high-strength concrete with low w/c or w/b ratios occurs a few days after casting (JCI, 1996; Principgallo *et al.*, 2003).

Hydration heat and autogenous shrinkage thus appear to be closely related. Moreover, the autogenous shrinkage of high-strength mass concrete is higher than that of a generally standardised $100 \times 100 \times 400$ mm specimen. Accordingly, it is thought that understanding the relationship between hydration heat and autogenous shrinkage at an early age is important in determining the complete process of autogenous shrinkage in high-strength mass concrete. However, this will not clearly explain the relationship between hydration heat and autogenous shrinkage at an early age, as there has not been any certain quantitative analysis of their history curves in previous studies.

If a method of analysis of the history curves of hydration temperature and autogenous shrinkage at an early age could be established, the relationship between the two could be elucidated. Such a method is presented in this study. Based on this method, the early-age properties and relationships between hydration heat and autogenous shrinkage in high-strength mass concrete with different mixture proportions are investigated.

Experiment

Experimental plan

The experimental conditions of the study are summarised in Table 1. Two different specimen sizes, $100 \times 100 \times 400$ mm and $300 \times 300 \times 300$ mm, were used. The $300 \times 300 \times 300$ mm specimens were prepared in a semi-adiabatic condition considering the insulation effect of mass concrete. Mixture proportions of the $300 \times 300 \times 300$ mm samples were varied to assess their influence on the early-age properties of hydration heat and autogenous shrinkage. The variations were an addition of 0·3% retarder and replacements of 30% fly ash (FA) and 50% ground granulated blast-furnace slag (GGBS).

	Specimen				
	$100^2 \times 400$-OPC*	$300^2 \times 300$-OPC	$300^2 \times 300$-RET(0·3)†	$300^2 \times 300$-FA(30)	$300^2 \times 300$-GGBS(50)
Size: mm	$100 \times 100 \times 400$	$300 \times 300 \times 300$	$300 \times 300 \times 300$	$300 \times 300 \times 300$	$300 \times 300 \times 300$
Curing	In air (20°C)	Semi-adiabatic	Semi-adiabatic	Semi-adiabatic	Semi-adiabatic
Admixture	—	—	0·3% retarder	30% FA	50% GGBS

* OPC: Ordinary Portland cement; † RET: Retarder

Table 1. Experimental conditions

Materials and mixture proportions

The mixture proportions of the high-strength concrete are shown in Table 2. The w/b was 0·2 and the unit weight of the binder was 800 kg/m^3. Details of the types and properties of the materials used are shown in Table 3.

Specimens and test methods

The specimens and test method are illustrated in Figure 1. The $300 \times 300 \times 300$ mm specimens were cast in moulds made of expanded polystyrene board of thickness 100 mm. To reduce friction between the concrete and the mould, a double layer of PVC film and Teflon film were used. The temperature and total shrinkage (autogenous shrinkage + thermal strain) of the $300 \times 300 \times 300$ mm specimens were measured continuously without removal of the mould. The mould of the $100 \times 100 \times 400$ mm specimen was removed 24 h after casting. The specimen was then wrapped in *PE* film and aluminium adhesive tape to prevent the moisture from moving. The inner temperature and the total shrinkage of the specimen were measured every 10 min after casting using a thermocouple and an embedded gauge.

Autogenous shrinkage of the $100 \times 100 \times 400$ mm specimen can be investigated while excluding thermal effects on the assumption of a quasi-isothermal condition (Aïtcin, 1999; Lee *et al.* 2002). However, because the temperature in the $300 \times 300 \times 300$ mm semi-adiabatic specimens increased greatly, the total measured shrinkage should be corrected for thermal strain. Accordingly, in this study, the total shrinkage was calculated using

$$1. \quad \varepsilon_{auto} = \varepsilon_{total} - \varepsilon_{thermal}$$

where ε_{auto} is the autogenous shrinkage ($\times 10^{-6}$), ε_{total} is the total measured stain ($\times 10^{-6}$) and $\varepsilon_{thermal}$ is the thermal strain ($\times 10^{-6}$). The thermal strain can be calculated from

$$2. \quad \varepsilon_{thermal} = \gamma \Delta t$$

where γ is the thermal expansion coefficient (TEC) of the specimen ($\times 10^{-6}$/°C) and Δt is the temperature change (°C).

The TEC of concrete varies according to the mixture proportions and materials. Moreover, it is difficult to evaluate the TEC of concrete at an early age since its phase and microstructure change with time. If the rise in temperature is sufficiently fast, the measured strain will only have a thermal origin (Loukili *et al.*, 2000). In this study, a ∅100 × 200 mm cylinder specimen with

Specimen	w/b	Slump flow: mm	S/a*	Unit weight: kg/m^3						Admixture: %	
				Water	OPC	FA	GGBS	Gravel	Sand	Retarder	HRWR†
$100^2 \times 400$-OPC	0·2	650 ± 50	0·47	160	800	0	0	781	664	0	1·0
$300^2 \times 300$-OPC	0·2	650 ± 50	0·47	160	800	0	0	781	664	0	1·0
$300^2 \times 300$-RET(0·3)	0·2	650 ± 50	0·47	160	800	0	0	781	664	0·3	1·1
$300^2 \times 300$-FA(30)	0·2	650 ± 50	0·47	160	560	240	0	730	620	0	1·0
$300^2 \times 300$-GGBS(50)	0·2	650 ± 50	0·47	160	400	0	400	766	651	0	0·8

* S/a : Sand-aggregate ratio
† HRWR : high-range water reducer

Table 2. Mixture proportions of concrete

Cement	Ordinary Portland cement
	Density 3·15 g/cm^3 Fineness 3770 cm^2/g
Fine aggregate	De-salting sand Maximum size 5 mm Density 2·54 g/cm^3 Fineness modulus 3·05 Absorption ratio 1·01%
Coarse aggregate	Crushed aggregate Maximum size 20 mm Density 2·65 g/cm^3 Fineness modulus 6·02 Absorption ratio 1·39%
FA	Density 2·13 g/cm^3 Fineness 2976 cm^2/g
GGBS	Density 2·91 g/cm^3 Fineness 4700 cm^2/g
Retarder	Gluconic acid type
High-range water reducer	Polycarboxylic acid type

Table 3. Materials

an embedded thermocouple and strain gauge was cast and immersed in a water bath as shown in Figure 2. The temperature of the bath was initially close to 20°C and the water was heated for 10 min. The temperature change (Δt) and the amount of expansion ($\Delta\varepsilon$) of the specimen were then measured and the TEC ($\Delta\varepsilon/\Delta t$) of the concrete calculated.

Analysis of history curves of hydration temperature and autogenous shrinkage

Based on previous studies (Horita and Nawa, 2001; Principallo *et al.*, 2003; Takahasi *et al.*, 1996), the history curve of autogenous shrinkage can be divided into three sections as shown in Figure 3. Swelling or autogenous shrinkage increases immediately after casting to reach the bend point or turning point (Takahasi *et al.*, 1996) (this is labelled i in Figure 3); it then increases rapidly after the bend point (ii). The rate of increase of autogenous shrinkage then gradually decreases and converges to a final value (iii).

The history curve of the hydration temperature (also shown in Figure 3) clearly consists of four sections. At first, temperature gradually increases (labelled I in Figure 3), it then rapidly increases (II), converges at a maximum temperature (III) and then gradually decreases (IV).

The most important sections of these curves are those in which hydration temperature and autogenous shrinkage increase rapidly (i.e. sections II and ii); these are referred to here as the hydration heating section (HHS) and the autogenous shrinking section (ASS) respectively. This study focuses on these sections to analyse the early-age properties of hydration temperature and autogenous shrinkage, in particular the linear slopes of the sections (the HHV and the autogenous shrinking velocity (ASV)). The terms used in this paper to analyse the properties of the HHS and ASS are shown in Table 4.

To set the HHS and calculate the linear slope of the history curve of the actual hydration temperature, a statistical method of regression was carried out. In this way, the calculated regression coefficient is the linear slope. If the section on which regression is applied is not set clearly or if a datum point is not set, analysis will be difficult and calculation of the HHV of each temperature history curve will lack consistency. Therefore, first of all, it is

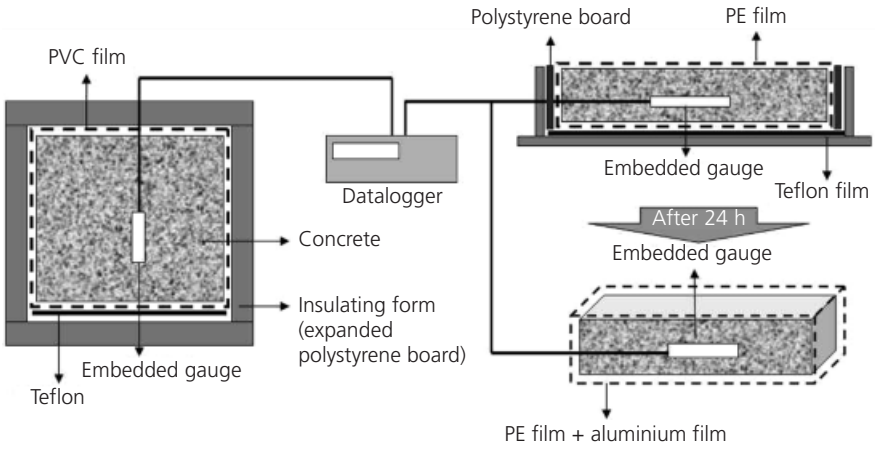

Figure 1. Test method for hydration temperature and autogenous shrinkage

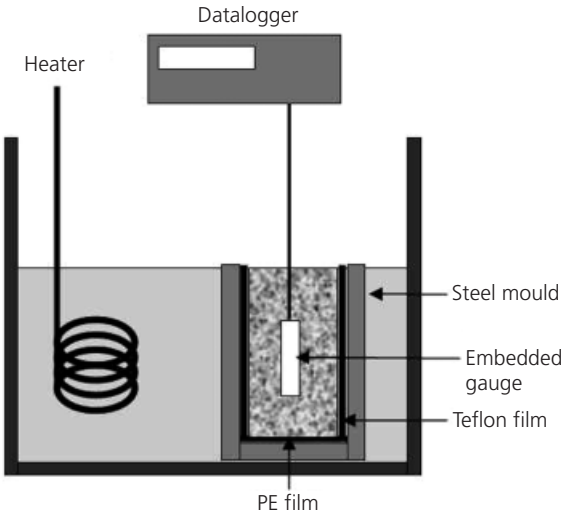

Figure 2. Test method for TEC of concrete

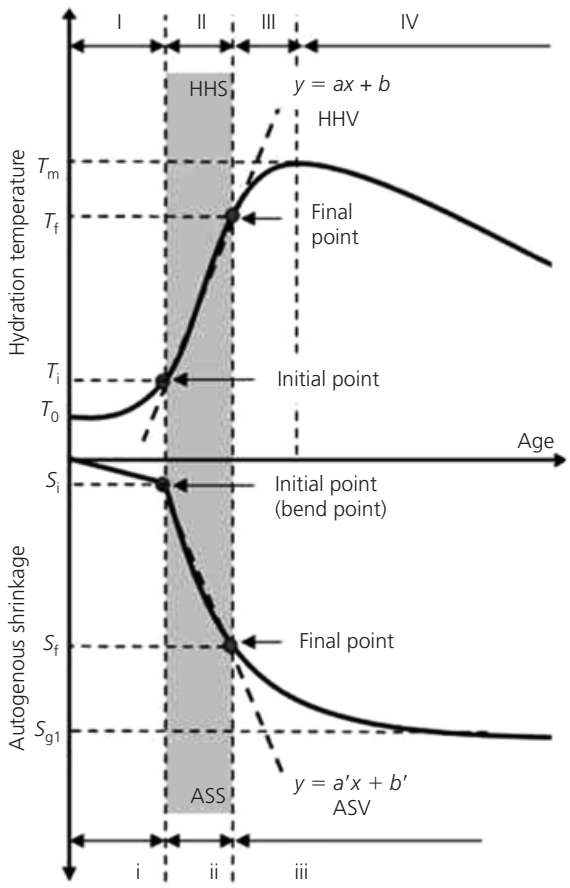

Figure 3. History curves of hydration temperature and autogenous shrinkage

necessary to explain the method to determine the point at which to set the section.

The datum point of a section was determined by applying the adiabatic temperature equation, which is shown in Figure 4. The temperature history curve estimated by means of the adiabatic temperature equation can be divided into three sections – where hydration temperature increases rapidly, where the temperature converges at the maximum temperature and where the maximum temperature is constant. That is, typical forms of sections II and III of the actual hydration temperature history curve can be found in the adiabatic temperature curve. The final point of the HHS, which has a fixed coefficient for determination, can thus be calculated from this curve. This study makes the assumption that the form of the initial point of the HHS (t_1, T_1) to the maximum temperature point (t_3, T_3) in the actual hydration temperature history curve is identical to that from the starting point (t_1', T_1') to the maximum temperature point (t_3', T_3') of the adiabatic temperature curve.

A regression was subsequently performed with adiabatic temperature history curves drawn for the conditions shown in Table 5. The final point (t_2', T_2') was calculated with a determination coefficient that was more than 0·95 from the starting point. The relationships between the temperature of the final point (T_2') and the maximum adiabatic temperature rise (T_3') were then analysed. As a result (Figure 5) it was confirmed through the regression equation that T_2'/T_3' with a determination coefficient of 0·95 was 0·80. Therefore, in adiabatic temperature history curves that occur under the above conditions, the final point of the HHS that represents 95% accuracy as regards the regression equation is the point at 80% of the maximum temperature rise.

When the HHS and HHV with a determination coefficient that exceeds 0·95 in the actual hydration temperature history curve are calculated, the analytical principle of the adiabatic temperature history curve explained above can be applied inversely. This can be summarised as

(*a*) set the final point (t_2, T_2) of the HHS (the point at 80% of the maximum temperature rise)
(*b*) based on the final point, run regression analysis and review determination coefficient
(*c*) set the initial point (t_1, T_1) of HHS and calculate the HHV.

In terms of autogenous shrinkage, after setting a bend point as the initial point of the ASS, the regression is performed. If a clear bend point does not exist, as with the HHS, after the final point is set (the point at 80% of autogenous shrinkage at 91 days) regression analysis is conducted.

Results and discussion

Measurement of hydration temperature and analysis

Figure 6 shows the hydration temperature history curves for the specimens studied in this work (see Table 1 for details of

	Definition and calculation methods
HHS	
Temperature rise	Amount of temperature increase during HHS Rise $= T_f - T_i$
Temperature rise ratio	Proportion of temperature rise to maximum temperature rise Ratio $= \dfrac{T_f - T_i}{T_m - T_0} \times 100$
Hydration heating velocity (HHV)	Linear slope of HHS Regression coefficient a
ASS	
Shrinkage rise	Amount of autogenous shrinkage increase during ASS
Shrinkage rise ratio	Proportion of autogenous shrinkage rise to autogenous shrinkage at 91 days
Autogenous shrinking velocity (ASV)	Linear slope of ASS Regression coefficient a'

Table 4. Factors for HHS and ASS analysis

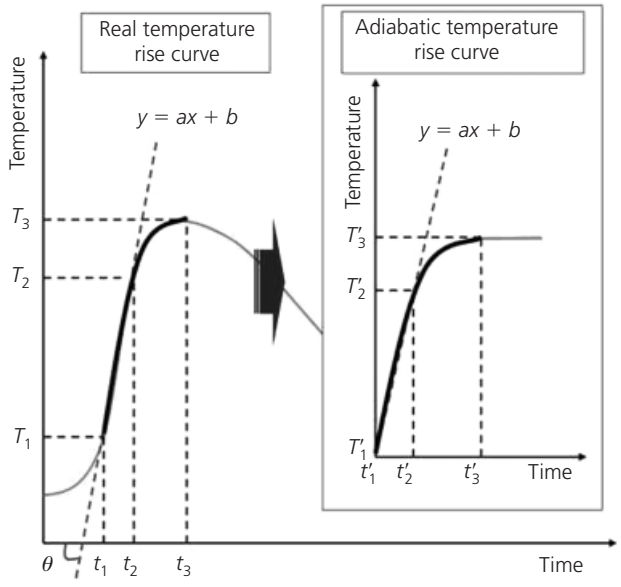

Figure 4. Application of adiabatic temperature rise curve for calculation of HHS and HHV

specimens). The maximum temperature of specimen $300^2 \times 300$-OPC (73°C) was approximately 2·3 times higher than that of $100^2 \times 400$-OPC (32°C). The maximum temperatures of specimens $300^2 \times 300$-RET(0·3), $300^2 \times 300$-FA(30) and $300^2 \times 300$-GGBS(50) were 67·7, 64·2 and 64·8, respectively, approximately 7–10% less than $300^2 \times 300$-OPC. These reductions in temperature can be attributed to the hydration delay effect caused by the retarder and the dilution effect in the cement content due to the use of FA and GGBS.

Table 6 shows the HHS analysis results and Figure 7 shows the hydration temperature rise and rise ratio to maximum temperature in the HHS. In this study, hydration temperature rise ratios of the HHS according to specimen size and mixture proportions were in the range 70–80%. The HHV of specimen $300^2 \times 300$-OPC (9·90°C/h) was more than six times larger than that of $100^2 \times 400$-OPC (1·59°C/h). The HHV values of $300^2 \times 300$-RET(0·3), $300^2 \times 300$-FA(30) and $300^2 \times 300$-GGBS(50) were calculated as 8·01, 4·73 and 3·88, respectively (the latter two thus being less than 50% of the value for specimen $300^2 \times 300$-OPC).

TEC measurements and correction by maturity

Initially, the temperature change and the amount of expansion were measured via a TEC test, as shown in Figure 2, and the TEC values were calculated from them. Based on the measured TEC values with time, a TEC history curve could be calculated by regression. However, these results were obtained from the ∅100 × 200 mm cylinder specimen, which had a low temperature. In the case of the 300 × 300 × 300 mm semi-adiabatic specimens, the TEC and the concrete phase changed more quickly than the ∅100 × 200 mm cylinder specimen due to the high temperature of the former (Teramoto and Maruyama, 2008). The maturity method is very useful here. The concept of maturity makes it possible to estimate the degree of advancement of the hydration reactions corresponding to concrete hardening (Turcry *et al.*, 2002; Waller *et al.*, 2004). In this study, to determine a more exact TEC value for the 300 × 300 × 300 mm semi-

Adiabatic temperature equation*	Type of cement	Unit weight of cement: kg/m^3	Placement temperature: °C	Measurement interval: min
$Q(t) = Q_\infty(1 - e^{-\alpha t})$	OPC	300, 400, 500, 600, 700, 800, 900, 1000	10, 20, 30	10

* $Q(t)$, adiabatic temperature at age t (°C); $Q\infty$, maximum adiabatic temperature rise (°C); α, coefficient for adiabatic temperature rise velocity; t, age (days)

Table 5. Analysis conditions of adiabatic temperature rise curves

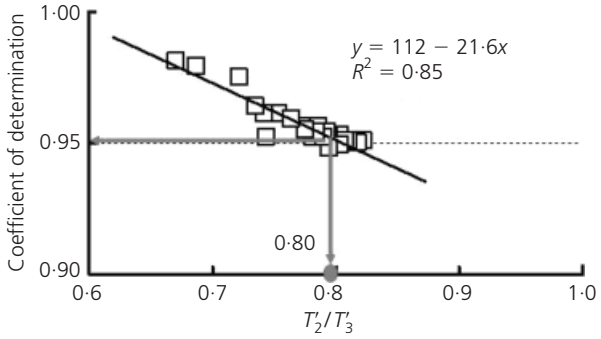

Figure 5. Relation between T'_2/T'_3 and coefficient of determination

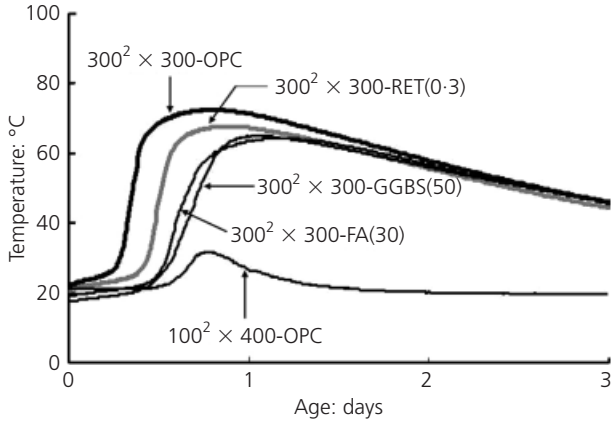

Figure 6. History curves of hydration temperature

	Initial point		Final point		Regression equation	HHV: °C/h	Duration: h	Maximum temperature rise: °C
	Time: h	Temp.: °C	Time: h	Temp.: °C				
$100^2 \times 400$-OPC	11·5	21·3	16·7	29·7	$y = 1{\cdot}91 + 1{\cdot}59x$	1·59	5·2	10·7
$300^2 \times 300$-OPC	5·5	25·8	9·7	62·5	$y = -34{\cdot}7 + 9{\cdot}90x$	9·90	4·17	51·0
$300^2 \times 300$-RET(0·3)	8·7	25·0	13·3	58·8	$y = -50{\cdot}2 + 8{\cdot}01x$	8·01	4·67	47·1
$300^2 \times 300$-FA(30)	9·2	21·8	17·2	55·1	$y = -27{\cdot}6 + 4{\cdot}73x$	4·73	8·00	45·5
$300^2 \times 300$-GGBS(50)	9·0	20·3	18·5	55·1	$y = -19{\cdot}7 + 3{\cdot}84x$	3·88	9·50	47·4

Table 6. Results of analysis of HHS

adiabatic specimens, the TEC history calculated by regression was corrected by the maturity method.

Figure 8 shows the results when the TEC was corrected by maturity. The TEC values of specimen $100^2 \times 400$-OPC and the ∅100 × 200 mm cylinder were nearly identical because their temperatures were similar. The TEC value of $100^2 \times 400$-OPC decreased slowly but then, nearly 7 h after casting, decreased rapidly. Finally, it converged to $9{\cdot}5 \times 10^{-6}$/°C nearly 16 h after casting. The TEC value of $300^2 \times 300$-OPC showed a similar trend, decreasing rapidly approximately 6 h after casting and converging about 10 h after casting. The TEC of $300^2 \times 300$-RET(0·3) behaved in a manner similar $300^2 \times 300$-OPC, converging to $10{\cdot}2 \times 10^{-6}$/°C about 30 h after casting.

For $300^2 \times 300$-FA(30) and $300^2 \times 300$-GGBS(50), TEC values increased rapidly after casting, and then decreased rapidly 6 and 5 h after casting, respectively. The values converged to 8×10^{-6}/°C

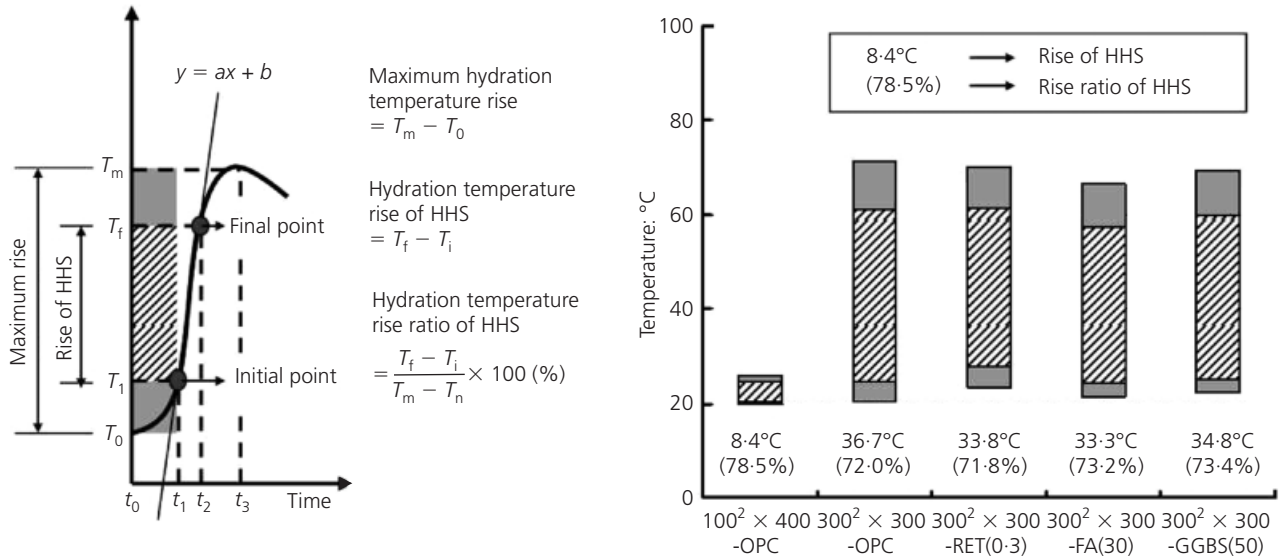

Figure 7. Hydration temperature rise and rise ratio to maximum temperature in the HHS

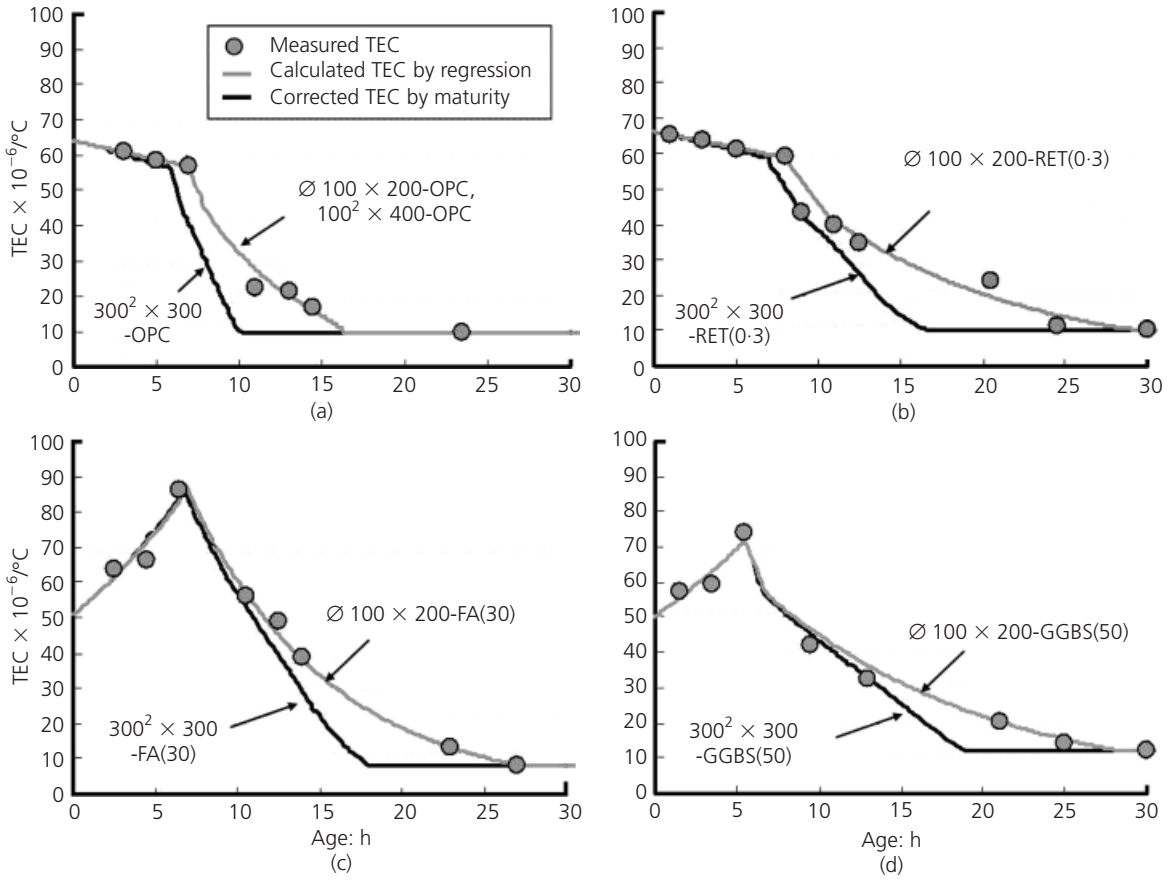

Figure 8. Thermal expansion coefficients for (a) OPC, (b) RET-0·3, (c) FA-30 and (d) GGBS-50

and 12×10^{-6}/°C, respectively, about 18 and 19 h after casting. Based on these corrected TEC values, autogenous shrinkage was separated from total measured strain.

Separation of autogenous shrinkage and analysis

To separate autogenous shrinkage from the total measured strain, it is necessary to calculate the thermal strain from the TEC values and temperature. Thermal strain was calculated from Equation 3, as proposed by Loukili *et al.* (2000)

$$\varepsilon_{\text{thermal}}(n) = \varepsilon_{\text{thermal}}(n-1) + \left[[T(n) - (T(n-1)]\left(\frac{\gamma(n) + \gamma(n-1)}{2}\right)\right] \quad (3)$$

where $\varepsilon_{\text{thermal}}(n)$ is thermal strain, $T(n)$ is temperature and $\gamma(n)$ is TEC at time n. The autogenous shrinkage was calculated by subtracting the thermal strain from the total measured strain.

Figure 9 shows the history of total measured strain, thermal strain and autogenous shrinkage. Autogenous shrinkage at 91 days for $100^2 \times 400$-OPC was -324×10^{-6} (Figure 9(a)), compared with (-1550×10^{-6}) for specimen $300^2 \times 300$-OPC (Figure 9(b)). These results indicate that, although the specimens had the same mixture proportions, as the inner temperature of the specimen increased, autogenous shrinkage increased. Some reasons for the differences in autogenous shrinkage with inner temperature can be found in the studies of Lothenbach *et al.* (2007, 2008), who reported that a higher curing temperature led to precipitation of a denser inner calcium silicate hydrate (C–S–H), decrease of the ettringite content at 40°C and above, and differences in the morphology of the precipitating ettringite (very short needles at 40°C). These phenomena can lead to an increase in shrinkage.

Autogenous shrinkage at 91 days for $300^2 \times 300$-RET(0·3), $300^2 \times 300$-FA(30) and $300^2 \times 300$-GGBS(50) specimens was -1461×10^{-6}, -1376×10^{-6} and -1382×10^{-6}, respectively, 6–11% smaller than that of $300^2 \times 300$-OPC.

It has been reported that autogenous shrinkage is significantly reduced in concrete with the addition of FA (Chan *et al.*, 1998; Lee *et al.*, 2003), a result supported in this study of specimen $300^2 \times 300$-FA(30). However, when FA with a very much smaller average particle size than cement was used, greater autogenous shrinkage was found (Tangtermsirikul, 1998; Wang *et al.*, 2001). In addition, Termkhajornkit *et al.* (2005) reported that autogenous shrinkage increased when the replacement level of FA was 25%.

In the case of concrete containing GGBS, autogenous shrinkage increases as the percentage of cement substituted by GGBS increases up to 90% (Tazawa and Miyazawa, 1999). The use of GGBS gives concrete a finer pore structure and contributes to a lower relative humidity, which increases the degree of self-desiccation within the cement paste (Roy and Idorn, 1982). However, in this study, autogenous shrinkage of the $300^2 \times 300$-GGBS(50) specimen showed a dissimilar result. Lim and Wee (2000) reported that a high replacement of GGBS induced a reduction in autogenous shrinkage. In their research, the 80% GGBS concrete showed the lowest autogenous shrinkage among the GGBS concretes they investigated.

A pozzolanic reaction largely depends on temperature (Hanebara *et al.*, 2001). Young (1988) reported that the pore size distribution was strongly influenced by the curing temperature: a high temperature increased the volume of mesopores. Aldea *et al.* (2000) reported that 50% replacement of GGBS led to the highest proportion of coarser pores. They also found that the volume of coarse pores increased as curing temperature was increased. In this study, the $300^2 \times 300$-GGBS(50) specimen underwent a high-temperature process. The high temperature may have caused an increase in the volume of coarse pores and a reduction in capillary pore pressure, which can lead to a reduction in the amount of autogenous shrinkage. Studies of the effects of FA and GGBS on the autogenous shrinkage of high-strength mass concrete are very rare and further experimental research is required.

Table 7 shows the results of ASS analysis and Figure 10 shows autogenous shrinkage rise and shrinkage ratio at 91 days. The ASS shrinkage ratio of the $100^2 \times 400$-OPC specimen was lower than that of $300^2 \times 300$-OPC. In the semi-adiabatic specimens, all ASS shrinkage ratios were close to 50–60%. Additionally, for concrete with admixtures (i.e. RET(0·3), FA(30) and GGBS(50)), the autogenous shrinkage rise of ASS was lower than that of the $300^2 \times 300$-OPC specimen.

The ASV of the $100^2 \times 400$-OPC specimen was $-9{\cdot}4 \times 10^{-6}$/h; that of $300^2 \times 300$-OPC was approximately 28 times higher $(-267 \times 10^{-6}$/h). The ASV values of $300^2 \times 300$-RET(0·3), $300^2 \times 300$-FA(30) and $300^2 \times 300$-GGBS(50) were -218×10^{-6}/h, -140×10^{-6}/h and -81×10^{-6}/h, respectively (i.e. around 80, 50 and 30% of that of $300^2 \times 300$-OPC).

Relationship between hydration temperature and autogenous shrinkage

Figure 11 shows the relationship between HHV and ASV. Although this plot takes into account the $300^2 \times 300$-FA(30) and $300^2 \times 300$-GGBS(50) specimens, a linear tendency can clearly be seen – a higher HHV results in a higher ASV.

Figure 12 shows the relationship between HHV and autogenous shrinkage at 91 days. In the case of concrete mixed with only OPC ($100^2 \times 400$-OPC, $300^2 \times 300$-OPC and $300^2 \times 300$-RET(0·3)) as a binder without FA and GGBS, as HHV increased, autogenous shrinkage at 91 days also increased. It was found that a higher HHV of concrete at an early age led to greater ultimate autogenous shrinkage. Considering this correlation, for concrete containing FA or GGBS, the change in the amount of ultimate autogenous shrinkage according to the HHV change can be greater than that observed with OPC.

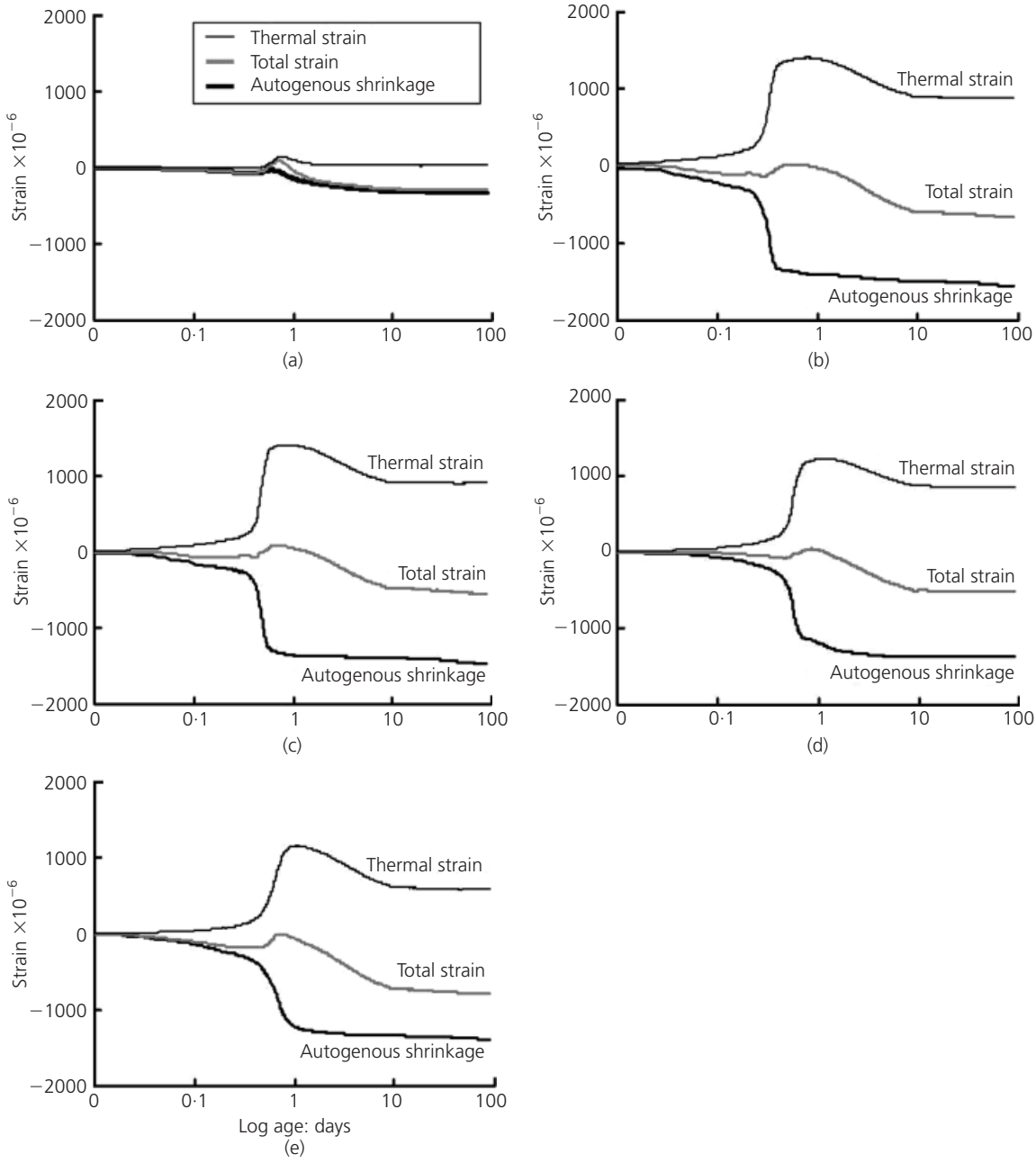

Figure 9. History curves of total strain, thermal strain and autogenous shrinkage for (a) $100^2 \times 400$-OPC, (b) $300^2 \times 300$-OPC, (c) $300^2 \times 300$-RET(0·3), (d) $300^2 \times 300$-FA(30) and (e) $300^2 \times 300$-GGBS(50)

Some researchers have reported a correlation between autogenous shrinkage and maturity. Tazawa *et al.* (1994) and Hedlund and Jonasson (2000) investigated the effect of different curing temperatures on autogenous shrinkage and concluded that autogenous shrinkage could be simulated with the maturity concept. In this study, the relationships between maturity of the HHS and the properties of autogenous shrinkage were investigated. The base temperature for the maturity calculation was −10°C.

Figure 13 shows the relationship between the maturity of the HHS and the HHV. Except for specimen $100^2 \times 400$-OPC, the two factors are in inverse proportion to each other. The relationship between the maturity of the HHS and ASV shows a similar trend (Figure 14). Figure 15 shows the relationship between the maturity of the HHS and the amount of autogenous shrinkage at 91 days. Even in concrete mixed with only OPC as a binder, a clear tendency was not found. Figure 16 shows a clear

	Initial point		Final point		Regression equation	ASV: $\times 10^{-6}$/h	Duration: h	Shrinkage at 91 days: $\times 10^{-6}$
	Time: h	Shrinkage: $\times 10^{-6}$	Time: h	Shrinkage: $\times 10^{-6}$				
$100^2 \times 400$-OPC	16·7	−17	31·8	−166	$y = 117 - 9{\cdot}40x$	−9·4	15·2	−309
$300^2 \times 300$-OPC	5·2	−332	8·8	−1243	$y = 1169 - 267x$	−267·0	3·7	−1550
$300^2 \times 300$-RET(0·3)	8·5	−296	12·8	−1166	$y = 1683 - 218x$	−218·0	4·3	−1461
$300^2 \times 300$-FA(30)	9·5	−277	15·2	−1015	$y = 1149 - 140x$	−140·0	5·7	−1376
$300^2 \times 300$-GGBS(50)	10·0	−383	19·7	−1109	$y = 477 - 81{\cdot}6x$	−81·6	9·7	−1382

Table 7. Results of analysis of ASS

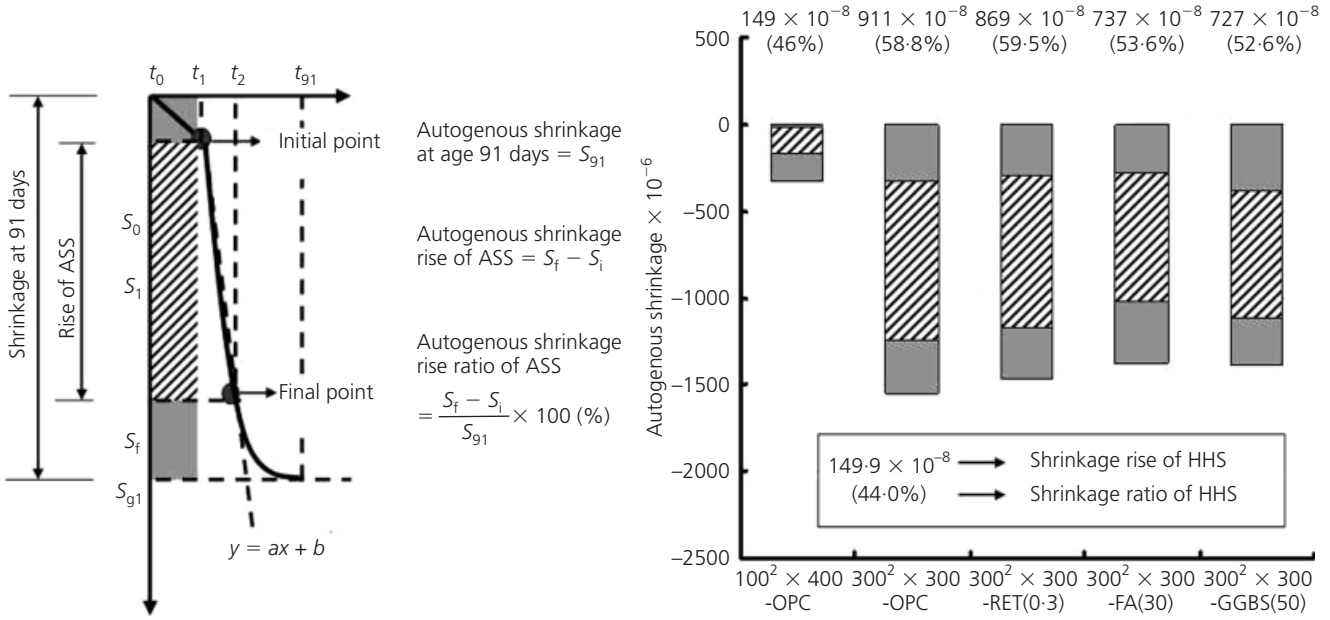

Figure 10. Autogenous shrinkage rise of ASS and shrinkage ratio to autogenous shrinkage at 91 days

relationship between HHV × maturity and autogenous shrinkage at 91 days – higher HHV × maturity led to greater autogenous shrinkage. This relationship shows a better correlation than that between the HHV and autogenous shrinkage.

Based on these relationships, it can be suggested that the ultimate amount of autogenous shrinkage can be decreased by controlling the HHV and can be predicted by analysing the HHV of high-strength mass concrete at an early age. Further experimental research and data analysis are necessary.

Conclusion

(*a*) It is possible to calculate the TEC of high-strength mass concrete using the maturity method and to separate autogenous shrinkage by subtracting the thermal strain calculated with the TEC from the total measured strain. The method proposed in this study made it possible to analyse the history curves of hydration temperature and autogenous shrinkage.

(*b*) The hydration temperature and HHV of concrete increased as the size of the specimen increased and decreased when the concrete contained a retarder, FA or GGBS.

(*c*) The TEC of concrete mixed with only OPC as a binder decreased slowly after casting. In addition, at a specific point, it decreased rapidly and finally converged. However, in the case of concrete containing FA and GGBS, the TEC increased rapidly after casting and decreased rapidly at a specific point.

(*d*) Even in the same mixture proportion, autogenous shrinkage becomes greater as the inner temperature increases. Autogenous shrinkage of high-strength mass concrete containing FA and GGBS is lower than that of OPC high-strength mass concrete. The ASV of concrete increased as the

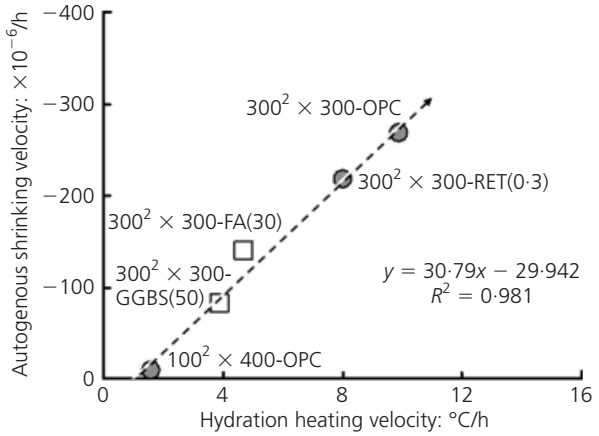

Figure 11. Relation between HHV and ASV: w/b = 0·2; binder = 800 kg/m^3

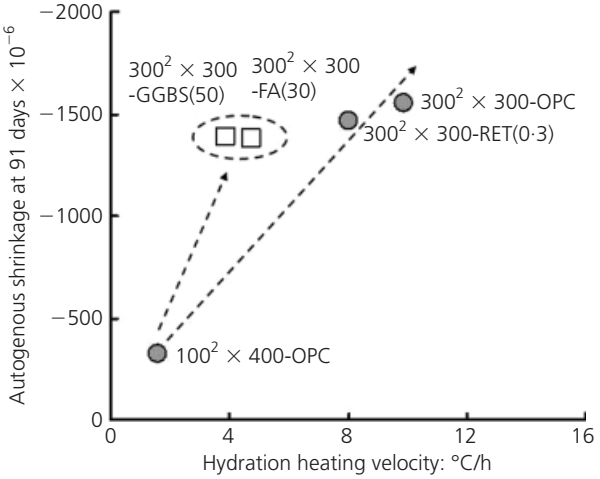

Figure 12. Relation between HHV and autogenous shrinkage at 91 days: w/b = 0·2; binder = 800 kg/m^3

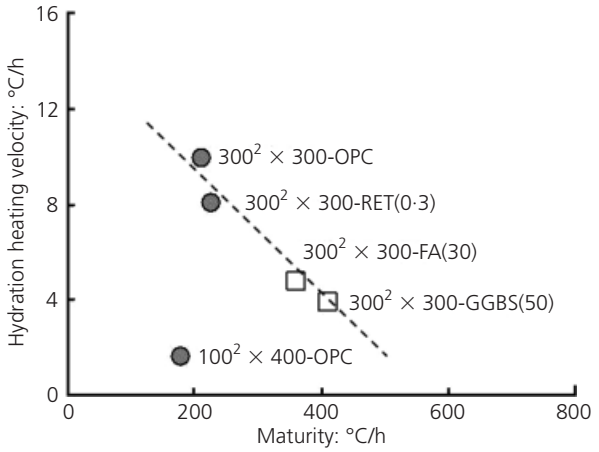

Figure 13. Relation between maturity of HHS and HHV: w/b = 0·2; binder = 800 kg/m^3

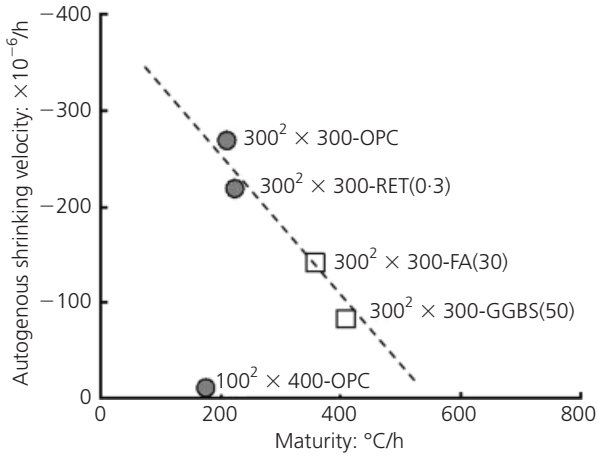

Figure 14. Relation between the maturity of HHS and ASV: w/b = 0·2; binder = 800 kg/m^3

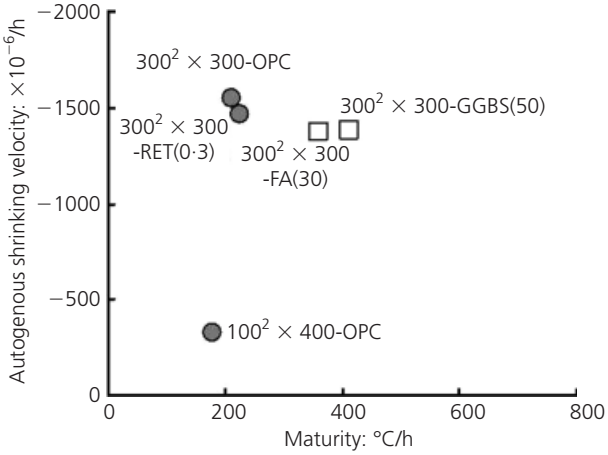

Figure 15. Relation between maturity of HHS and autogenous shrinkage at 91 days: w/b = 0·2; binder = 800 kg/m^3

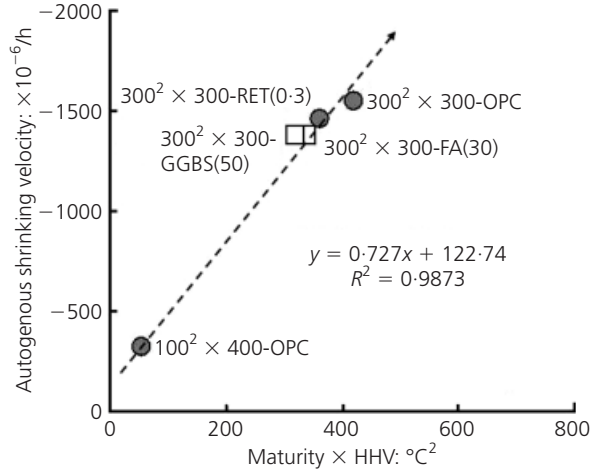

Figure 16. Relation between maturity × HHV and autogenous shrinkage at 91 days: w/b = 0·2; binder = 800 kg/m^3

size of the specimen increased and decreased when the concrete contained a retarder, FA or GGBS.

(*e*) There was a close correlation between hydration temperature and autogenous shrinkage at an early age
  (*i*) a higher HHV corresponds to a higher ASV and greater autogenous shrinkage
  (*ii*) a higher HHV × maturity factor results in greater autogenous shrinkage.

Acknowledgements

This work was supported by a Korea Science and Engineering Foundation (KOSEF) grant funded by the Korean government (MEST) (R01-2007-000-11142-0, 2009-0052476). Some researchers were supported by Brain Korea 21, also funded by the Korean government.

REFERENCES

Aïtcin PC (1999) Autogenous shrinkage measurement. In *Autogenous Shrinkage of Concrete* (Tazawa E (ed.)). E&FN Spon, London, pp. 257–268.

Aldea CM, Young F, Wang K and Shah SP (2000) Effects of curing conditions on properties of concrete using slag replacement. *Cement and Concrete Research* **30(3)**: 465–472.

Bjøntegaard Ø, Sellevold EJ and Hammer TA (1997) High performance concrete at early ages: selfgenerated stresses due to autogenous shrinkage and temperature. *Proceedings of International Seminar on Self-desiccation and its Importance in Concrete Technology, Lund*, pp. 1–7.

Chan YW, Liu CY and Lu YS (1998) Effect of slag and fly ash on the autogenous shrinkage of high performance concrete. *Proceedings of International Workshop on Autogenous Shrinkage of Concrete, Hiroshima*. JCI, Hiroshima, pp. 221–228.

Hanebara S, Tomosawa F, Kobayakawa M and Hwang KR (2001) Effects of water/powder ratio, mixing ratio of fly ash, and curing temperature on pozzolanic reaction of fly ash in cement paste. *Cement and Concrete Research* **31(1)**: 31–39.

Hedlund H and Jonasson JE (2000) Effect on stress development of restrained thermal and moisture deformation. *Proceedings of Shrinkage 2000, International RILEM Workshop on Shrinkage of Concrete, Paris*. RILEM, Cachan, pp. 355–375.

Horita T and Nawa T (2001) A study on autogenous shrinkage of cement mixes. *Journal of Structure and Construction Engineering* **542**: 9–15.

JCI (Japan Concrete Institute) (1996) *Technical Committee Report on Autogenous Shrinkage of Concrete*. JCI, Tokyo, pp. 114–122.

Lee HK, Im JY, Lee KM and Kim BG (2002) Autogenous shrinkage of high performance concrete containing fly ash. *Journal of the Korea Concrete Institute* **14(2)**: 249–256.

Lee HK, Lee KM and Kim BG (2003) Autogenous shrinkage of high-performance concrete containing fly ash. *Magazine of Concrete Research* **55(6)**: 507–515.

Lim SN and Wee TH (2000) Autogenous shrinkage of ground-granulated blast-furnace slag concrete. *ACI Materials Journal* **91(67)**: 587–593.

Lothenbach B, Winnefeld F, Alder C, Wieland E and Lunk P (2007) Effect of temperature on the pore solution, microstructure and hydration products of Portland cement pastes. *Cement and Concrete Research* **37(4)**: 483–491.

Lothenbach B, Matschei T, Möschner G and Glasser FP (2008) Thermodynamic modeling of the effect of temperature on the hydration and porosity of Portland cement. *Cement and Concrete Research* **38(1)**: 1–18.

Loukili A, Chopin D, Khelidj A and Touzo JL (2000) A new approach to determine autogenous shrinkage of mortar at an early age considering temperature history. *Cement and Concrete Research* **30(6)**: 915–922.

Lura P, Jensen OM and Breugel KV (2003) Autogenous shrinkage in high-performance cement paste: an evaluation of basic mechanisms. *Cement and Concrete Research* **33(2)**: 223–232.

Principallo A, Lura P, Breugel KV and Levita G (2003) Early development of properties in a cement paste: a numerical and experimental study. *Cement and Concrete Research* **33(7)**: 1013–1020.

Roy DM and Idorn GM (1982) Hydration, structure and properties of blast-furnace slag cements, mortars, and concrete. *ACI Journal* **79(6)**: 444–457.

Shima T, Matsuda T, Koide T, *et al.* (2006) Autogenous shrinkage characteristic of ultra high-strength concrete cured under high temperature. Part 1. Experimental result and shrinkage decrease effect by expansive admixture). *Proceedings of the Architectural Research Meeting of AIJ, Yokohama, Japan*, Architectural Institute of Japan, Tokyo, pp. 69–70.

Takahasi T, Nakata H, Yoshida K and Goto S (1996) Influence of hydration on autogenous shrinkage of cement paste. *Concrete Research and Technology* **7(2)**: 137–142.

Tangtermsirikul S (1998) Effect of chemical composition and particle size of fly ash on autogenous shrinkage of paste. *Proceedings of International Workshop on Autogenous Shrinkage of Concrete, Hiroshima*. JCI, Hiroshima, pp. 175–189.

Tazawa E and Miyazawa S (1999) Effect of constituents and curing condition on autogenous shrinkage of concrete. *Proceedings of International Workshop on Autogenous Shrinkage of Concrete, London*. E&FN Spon, London, pp. 267–280.

Tazawa E, Matsuoka Y, Miyazawa S and Okamoto S (1994) Effect of autogenous shrinkage on self stress in hardening concrete. *Proceedings of International Symposium on Thermal Cracking in Concrete at Early Ages, Munich*. Rilem, Bagneux, France, pp. 221–228.

Teramoto A and Maruyama I (2008) Temperature dependency of autogenous shrinkage of silica fume concrete with low W/B ratio. *Journal of Structure and Construction Engineering* **73(634)**: 2069–2076.

Termkhajornkit P, Nawa T, Nakai M and Saito T (2005) Effect of fly ash on autogenous shrinkage. *Cement and Concrete Research* **35(3)**: 473–482.

Turcry P, Loukili A, Barcelo L and Casabone JM (2002) Can the

maturity concept be used to separate the autogenous shrinkage and thermal deformation of a cement paste at early age? *Cement and Concrete Research* **32(9)**: 1443–1450.

Waller V, Aloia L, Cussigh F and Lecrux S (2004) Using the maturity method in concrete cracking control at early ages. *Cement and Concrete Composites* **26(5)**: 589–599.

Wang K, Shah SP and Phuaksuk P (2001) Plastic shrinkage cracking in concrete materials-influence of fly ash and fibers. *ACI Materials Journal* **98(49)**: 458–464.

Young JF (1988) A review of pore structure of cement paste and concrete and its influence on permeability. ACI Special Publication **108-1**: 1–18.